

Quantum Otto heat-engine with Kitaev-Heisenberg cluster: Possible roles of frustration, magnons, and duality

Sheikh Moonsun Pervez ^{1, 2, *} and Saptarshi Mandal ^{1, 2, †}

¹ Institute of Physics, Sachivalaya Marg, Bhubaneswar-751005, India

² Homi Bhabha National Institute, Training School Complex, Anushakti Nagar, Mumbai 400094, India

(Dated: January 8, 2026)

We study the performance of Kitaev-Heisenberg (KH) clusters as working media realizing a quantum Otto engine (QOE). An external Zeeman field with linear time dependency is used as the driving mechanism. The efficiency strongly depends on Kitaev (κ) and Heisenberg (J) exchange interaction. Interestingly, efficiency is comparable when the relative magnitude of κ and J is the same but of opposite signs. The above results are explained due to a subtle interplay of frustration, quantum fluctuation, and duality of eigen-spectra for the KH system when both the signs of κ and J are reversed. The maximum efficiency is shown to be dynamically related to eigen-spectra forming discrete narrow bands, where total spin angular momentum becomes a good quantum number. We relate this optimum efficiency to the realization of weakly interacting magnons, where the system reduces to an approximate eigen-system of the external drive. Finally, we extend our study to the large spin Kitaev model and find a quantum advantage in efficiency for $S = 1/2$. The results could be of practical interest for materials with KH interactions as a platform for QOE.

I. INTRODUCTION

The rapid advancement of technology has made it possible to realize interesting quantum devices, including nano-sensors [1] and nano-magnetism [2], where the quantum effect is the key controlling mechanism. In this respect, recent studies on quantum heat engine (QHE) [3–9] and batteries [10–14] have revealed many aspects of thermodynamics [15–20] in small systems, where various quantum effects compete with the general rules of thermodynamics, and often results in counter intuitive outcome which is absent in macroscopic, classical heat engines. Compared to conventional heat engines, the working medium (WM) of QHE promises to be more versatile because of the possibility of greater control to manipulate quantum states of matter [21–26]. Along with the recent advancement of nano-science and low-temperature physics, the effect of quantum thermodynamics is inevitable, and it renders the study of QHE an important field of research in present days. Starting from the original proposal of QHE in the context of maser [27, 28], recent theoretical and experimental studies show remarkable advancement in understanding quantum thermodynamics at the small scale [29–34].

In this work, we study the quantum Otto engine (QOE) [35, 36] taking small Kitaev-Heisenberg (KH) clusters [37–41] as WM, and follow the Otto cycle [42]. Otto engines deliver better efficiency with less emission, and have potential applications ranging from small generators to large-scale industrial applications [43–46]. Initial works on QOE mainly considered non-interacting quantum systems such as harmonic oscillator, two or few

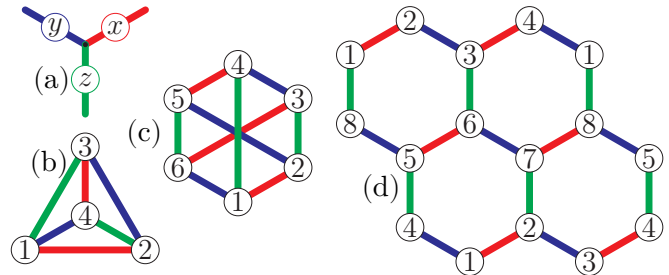


FIG. 1. (a) The red, blue, and green bonds indicate x - x , y - y , z - z -type interactions in Kitaev model. Panels (b), (c), and (d) depict the four, six, and eight-site clusters considered, respectively.

level atomic or spin systems, which have the convenience of analytical tractability [47–53]. The study on ideal quantum gas shows that, while ideal Bose gas exceeds the work and efficiency than that of classical ideal gas, ideal Fermi gas performs below classical limit [54–58]. However, these simple quantum systems mostly rely on single-particle quantum properties. To explore the true many-particle aspects in QOE performance, various studies have been recently carried out, such as one-dimensional Heisenberg-chain [59], Ising system [60, 61], XYZ-chain with DM interactions [62, 63], and one-dimensional Kitaev chains [64, 65]. All these studies reveal many interesting many-particle quantum aspects such as geometric friction [66], topological and finite-size effects [67], etc. Experiments on the realization of QOE [68–70] have also been achieved successfully, elucidating the concept of effective negative temperatures [68, 71].

The WM of this study, viz., the KH system, is one of the paradigmatic models exhibiting unique quantum state of matter, known as the quantum spin

* corresponding author, [✉ moonsun@iopb.res.in](mailto:moonsun@iopb.res.in)

† [✉ saptarshi@iopb.res.in](mailto:saptarshi@iopb.res.in)

liquid (QSL) [72–80]. Efforts of material realization of the Kitaev-QSL have progressed in positive direction in various Mott insulators [81–88], such as α -RuCl₃, Na₂IrO₃, Li₂IrO₃, etc. [89–93]. Here we discover interesting many-body effects of frustrated spin-system controlling the efficiency and work of the QOE for KH system. Our plan for the presentation is as follows.

In II A, we introduce the WM and briefly describe possible regimes of the system that are relevant to describing the performances of QOE. The four-stroke Otto-cycle is introduced in II B. The mathematical definition of efficiency and all possible operational modes that a QOE can perform are also mentioned. In III, we chart out the key results in various subsections. In III A, we introduce the relevant parameter spaces for the Kitaev clusters for all four different operational modes (engine, accelerator, heater, refrigerator), and characterize them in terms of some fictitious effective temperature. In III B, we describe the behavior of maximum efficiency achieved and how it depends on the external magnetic field and relative signs of Kitaev and Heisenberg interactions. We successfully relate this maximum efficiency and other key properties to some interesting many-body aspects, such as the bunching effect of eigen-spectrum and duality property of high energy and low energy spectrum of KH clusters when the sign of both these interactions is reversed. In III C, we show large spin- S Kitaev cluster performance as QOE and find that there is a quantum advantage, i.e., the efficiency decreases as S is increased. The same quantum advantage is found to be true even for pure Heisenberg interaction in a tri-coordinated cluster. We conclude in section IV.

II. MODEL AND METHOD

A. Hamiltonian

Kitaev clusters: The WM under consideration are KH clusters of size 4, 6, and 8-sites, as schematically shown in FIG. 1. Hamiltonian of the system can be written as [94–100],

$$H(t) = H_K + H_H - h(t) \sum_j S_j^z, \quad (1)$$

$$H_K = \kappa \sum_{\langle j,k \rangle} S_j^\alpha S_k^\alpha, \quad H_H = J \sum_{\langle j,k \rangle} \vec{S}_j \cdot \vec{S}_k, \quad \alpha = x, y, z. \quad (2)$$

Here \vec{S}_j denotes the spin 1/2 operator at site ‘ j ’. H_K and H_H are the (time-independent) Kitaev and Heisenberg interactions, respectively. The last term in Eq.(1) denotes the external driving Hamiltonian, and for simplicity, we consider a linear time dependency of $h(t)$. The index α in H_K denotes the α -type bonds used to enumerate Kitaev interactions [FIG. 1]. κ and J denote the isotropic Kitaev and Heisenberg interactions.

Positive κ or J indicates antiferromagnetic (AFM) interaction, and their negative values correspond to ferromagnetic (FM) coupling. In our study, all possible signs and relevant magnitudes of κ and J are considered.

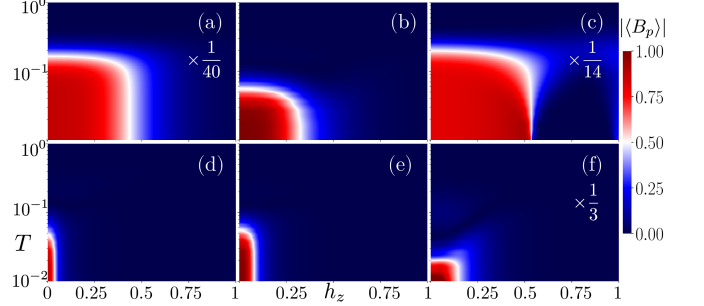


FIG. 2. $|\langle B_p \rangle|$ in magnetic field (h_z) - temperature (T) plane for 8-site cluster is plotted. The upper and lower panels are for the AFM and FM Kitaev model, respectively. Value of J is taken to be -0.3, 0, and 0.3 in panels (a,d), (b,e), and (c,f), respectively. For better visualization, panels (a), (c), and (f) have been scaled up; the actual data correspond to the colored data multiplied by the factor indicated in the respective panels.

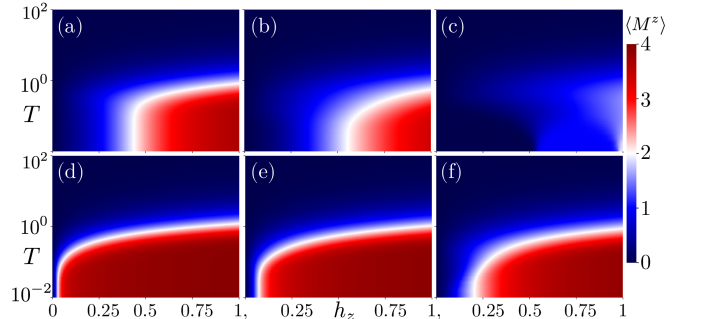


FIG. 3. Total magnetization $\langle M^z \rangle$ for 8-site cluster is plotted in $h_z - T$ plane. The upper and lower panels correspond to $\kappa = 1$ and $\kappa = -1$, respectively. Panels (a,d), (b,e), and (c,f) correspond to $J = -0.3, 0, 0.3$, respectively.

Brief description of possible regimes of Kitaev-Heisenberg clusters: Here we briefly describe the possible regimes that occur at different values of external Zeeman field, for various signs and magnitudes of κ and J . This will help us understand the dynamical aspects of various states of KH clusters that govern the QOE’s performance. We consider two relevant order parameters that are complementary to each other at different limits. The pure Kitaev Hamiltonian H_K hosts a QSL state in the thermodynamic limit. This QSL is characterized by short-range correlation, vanishing magnetization, conserved flux operator B_p , and spin-fractionalization [75, 101]. B_p is defined as the product of Kitaev Hamiltonian terms around a plaquette, and in our consideration, $B_p = \sigma_1^z \sigma_2^y \sigma_7^x \sigma_6^z \sigma_5^y \sigma_4^x$. On the other hand, the last two terms of Eq.(1) can be conveniently

characterized by magnetization $\langle M^z \rangle$.

In FIG. 2, comparison of panels (b) and (e) shows that $\langle B_p \rangle$ assumes a higher value (and close to 1), for a larger region for $\kappa = 1$ than $\kappa = -1$, which is found for a Kitaev system even in the 2D limit [102]. Addition of J rapidly decreases $\langle B_p \rangle$ of the AFM model, as seen in (a) and (c). On the other hand, inclusion of J for the FM model causes less decrement in comparison to the AFM one (panels (d) and (f)). A larger value of $\langle B_p \rangle$ corresponds to a proximate fractionalized phase with QSL state in the 2D limit. As we are dealing with clusters, we define this state as p-QSL, dubbed a ‘pro-quantum spin liquid state’. The p-QSL implies a possible realization of the QSL state in the thermodynamic limit. In FIG. 3, we plot $\langle M^z \rangle$ in $T - h_z$ plane, for the parameters same as in FIG. 2. There is a one-to-one correspondence of high $\langle B_p \rangle$ region to low $\langle M^z \rangle$ in the low temperature region. At high temperature, both quantities are vanishingly small, which denotes the usual paramagnetic phase in the 2D limit. As these small clusters qualitatively mimic the larger KH system very well, we predict the results of QOE shall remain similar for WM with more number of sites, which are difficult to access computationally, but may be relevant to potential applications in quantum technologies.

B. Quantum Otto cycle

Here we briefly describe the principle of QOE, as shown in FIG. 4. The Otto cycle involves a path $1 \rightarrow 2 \rightarrow 3 \rightarrow 4 \rightarrow 1$. The WM with initial Hamiltonian $H^{(1)}$ is made to equilibrate with a cold bath at temperature $T_c = 1/\beta_c$, to have energy $E^{(1)} = \text{Tr}(\rho^{(1)} H^{(1)})$, where $\rho^{(1)} = e^{-\beta_c H^{(1)}} / \text{Tr}(e^{-\beta_c H^{(1)}})$. Hamiltonian follows a unitary evolution $(1) \rightarrow (2)$, where the magnetic field is changed from h_2 to h_1 . This evolution is characterized by $U = \mathcal{T} \text{Exp} \left(-i \int_{h=h_2}^{h=h_1} H(t) dt \right)$. Thus at (2), before in contact to hot bath, density matrix $\rho^{(2)} = U \rho^{(1)} U^\dagger$, and energy $E^{(2)} = \text{Tr}(\rho^{(2)} H^{(2)})$. Next, WM is made to equilibrate with hot bath of temperature $T_h = 1/\beta_h$ and characterized by energy $E^{(3)} = \text{Tr}(\rho^{(3)} H^{(3)})$, where $\rho^{(3)} = e^{-\beta_h H^{(3)}} / \text{Tr}(e^{-\beta_h H^{(3)}})$. The system is then adiabatically evolved to (4) by $\tilde{U} = \mathcal{T} \text{Exp} \left(-i \int_{h=h_1}^{h=h_2} H(t) dt \right)$, after detaching from the hot bath. Heat exchanged during hot and cold thermalization processes, Q_h and Q_c respectively, and efficiency η , are defined as,

$$Q_h = E^{(3)} - E^{(2)}, Q_c = E^{(1)} - E^{(4)}, \eta = \frac{(Q_h + Q_c)}{Q_h}. \quad (3)$$

The work done during the cycle is defined as $\omega = -(Q_h + Q_c)$, using the sign convention of $+(-)$ when energy is absorbed (dissipated) by the WM. Depending on the property of WM, following Clausius inequality [70], QOE can operate in four modes: (i) heat-engine

[\mathcal{E}]: when $Q_h \geq 0, Q_c \leq 0, \omega \leq 0$, (ii) refrigerator [\mathcal{R}]: when $Q_h \leq 0, Q_c \geq 0, \omega \geq 0$, (iii) heat-accelerator [\mathcal{A}]: when $Q_h \geq 0, Q_c \leq 0, \omega \geq 0$, and (iv) heater [\mathcal{H}]: when $Q_h \leq 0, Q_c \leq 0, \omega \geq 0$. We note that these four operational modes can be explained in terms of energy diagram, and a fictitious effective temperature, which we define at any point on the Otto cycle as, $\text{Tr}(\rho(t) H(t)) = E(t) := \text{Tr}(H(t) e^{-\beta_{\text{eff}} H(t)}) / \text{Tr}(e^{-\beta_{\text{eff}} H(t)})$. $T_{\text{eff}} = 1/\beta_{\text{eff}}$ is a measure of how much an equilibrium temperature is required to equilibrate the Hamiltonian at time t to have the same energy as we get at that particular point of the Otto cycle. This indirectly measures the effect of the driving field, which changes the system’s internal energy.

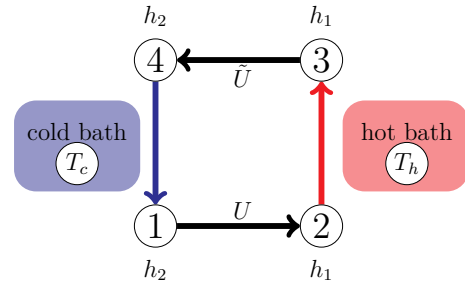
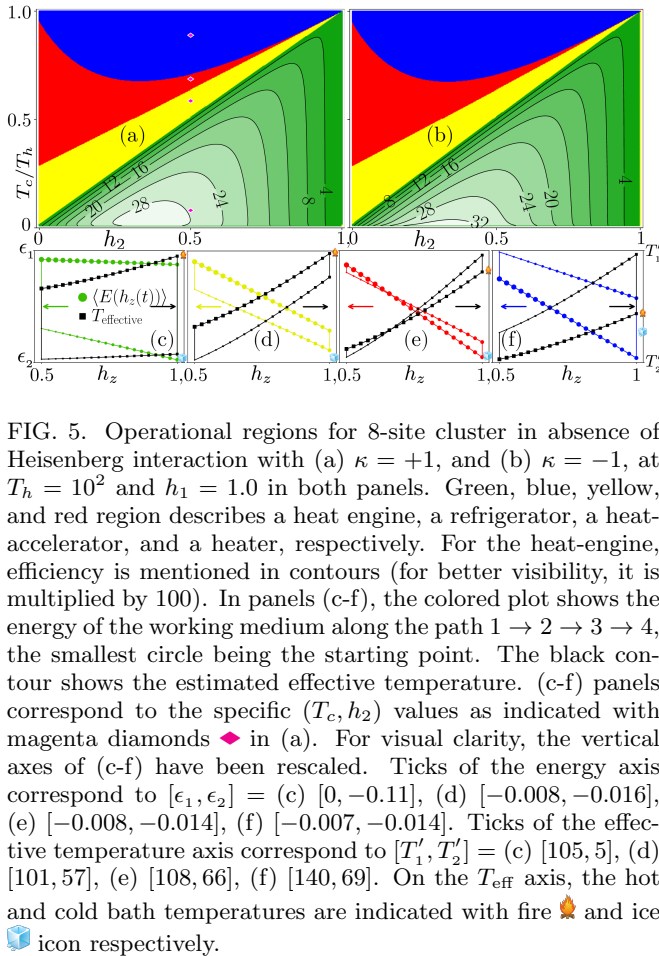


FIG. 4. Otto cycle is shown schematically. At (1), the system is described by the initial magnetic field h_2 and density matrix $\rho^{(1)}$, in equilibrium with cold-bath. The system is then detached from the cold bath and unitarily evolved to (2) with a magnetic field linearly increased up to h_1 , and characterized by a density matrix $\rho^{(2)}$. Now the system is brought in contact with a hot bath and described by a density matrix $\rho^{(3)}$. Finally, the system is detached from the hot bath and undergoes a unitary evolution to reach the state with h_2 with $\rho^{(4)}$ at (4).

We use the full exact diagonalization method to obtain these clusters’ energy spectra and eigenvectors. Using that, we calculate the density matrix, energy after each stroke, the amount of heat exchanged while attached to the thermal baths, and the work done on or by the system during two unitary processes. Following the Suzuki-Trotter decomposition, the unitary evolutions in two adiabatic paths $((1) \rightarrow (2), \text{ and } (3) \rightarrow (4))$ are obtained by discretizing the full time scale in small pieces and assuming the Hamiltonian to be constant during these short time intervals.

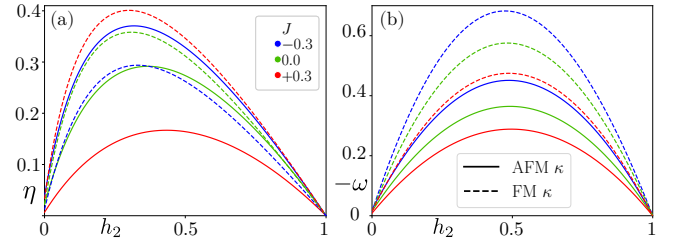
III. RESULTS

We chart out the different results in this section. Being qualitatively similar for all the clusters, we provide the results for the 8-site cluster only. The results tabulated here are obtained with $T_h = 10^2$ and $h_1 = 1$. Considering $\kappa = 5.5 \text{ meV}$ [88], these correspond to $T_h \sim 63 \text{ Kelvin}$, and $h_1 \sim 23 \text{ Tesla}$.



A. Working Regions

In FIG. 5, we show how the WM operates itself as \mathcal{H} , \mathcal{R} , \mathcal{A} , \mathcal{E} . The plots remain qualitatively unchanged in the presence of small J ; only the area of these modes in the parameter space changes. The performance of QOE in these modes can be described by the average energy $\langle E \rangle$, or the effective temperature T_{eff} as introduced before. We choose one representative point from each of these four modes (magenta diamonds \blacklozenge in FIG. 5a), and plot $\langle E \rangle$ and T_{eff} along the Otto cycle in FIG. 5(c-f). At low T_c , WM experiences \mathcal{E} . When T_c is increased, WM enters into \mathcal{A} mode, which is characterized by $\omega > 0$ which implies that $|Q_c| > |Q_h|$, while Q_h and Q_c remain positive and negative respectively. This indicates that for a given T_h , as one increases T_c , the thermal fluctuation enhances $|Q_c|$. When T_c is increased further, we enter into \mathcal{H} , where Q_h becomes negative in contradiction with \mathcal{E} and \mathcal{A} . It is caused by the effect of adiabatic pumping; the system's internal energy is changed to such an extent that the hot bath effectively becomes a sink. T_c is further increased to reach \mathcal{R} , where Q_c is positive, implying the WM is pumping out energy from the cold bath and transferring it to the hot one.



When we take sufficiently small h_1 to run the QOE deep inside the p-QSL region along the field axis [FIG. 2,3], vanishingly small efficiency and work are obtained, that too for high T_h only; so this is outside p-QSL along the temperature axis. If we restrict ourselves only to p-QSL (very low T_h , small h_1), the WM does not work as \mathcal{E} at all. All these indicate that there is no advantage in QOE due to the p-QSL. But this is even more interesting. That means a Kitaev candidate material, even if it fails to achieve the QSL due to the presence of other non-Kitaev interactions, can still be used as a QHE. In the following section, we show that the presence of some non-Kitaev (Heisenberg) interaction, which is unavoidable in real-world Kitaev materials, is not only acceptable but more desirable to build QOE. Interestingly, high temperature and large magnetic field are the suitable parameter space to achieve the QOE made with Kitaev WM, where $h_2 \lesssim h_1$ creates the \mathcal{E} mode, and $T_c \lesssim T_h$ generates the \mathcal{R} region.

B. Effect of Heisenberg interaction

As this work is primarily focused on the \mathcal{E} mode, we describe here the efficiency and work obtained in this mode, and present the effects of finite J . In FIG. 6, we see that the pure FM Kitaev model has a better efficiency than the pure AFM one. However, in both cases, when we introduce $|J| = 0.3$ with a sign opposite to that of κ , the efficiency increases. But, the work obtained is maximized (minimized) if the sign of J is $-(+)$, irrespective of κ . In search of the reason behind efficiency enhancement for competing κ and J , we pick h_2 values from FIG. 6a, at which the pure Kitaev WM produces the highest efficiency, and plot its variation for a range of $J : -1 \rightarrow +1$. The results are shown in FIG. 7(a,b) with $\kappa = \pm 1$ for different h_1 values.

It is remarkable that the plots are qualitatively symmetric when the signs of (κ, J) change together. Efficiency, in absence of J , attains maximum at $h_2 = 0.365$ and 0.31 , for $\kappa = \pm 1$. The obtained η are even more enhanced for a competing J , and become

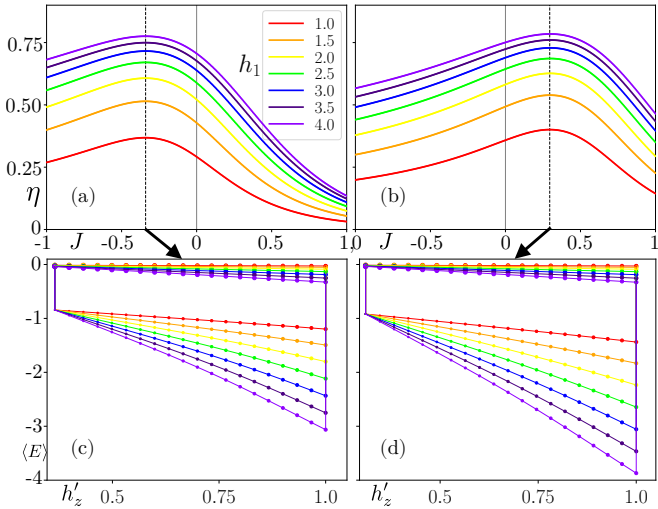


FIG. 7. Efficiency in (a) AFM and (b) FM Kitaev model for varying J , with $h_2 = 0.365$ and $h_2 = 0.31$ respectively, for different h_1 as in the legend box. Note that the peak of η remains at the same J points (dotted black lines) as we increase h_1 , and around these J points, narrow band formation of the eigen-states occurs, as shown in FIG. 8. In (c,d), we show the energy cycle at these maximum efficiency providing J points for AFM and FM Kitaev model, respectively, where the h_z axis is rescaled as $h'_z = h_2 + (1 - h_2) \frac{(h_z - h_2)}{(h_1 - h_2)}$ for better visual comparison. The point size increases as we walk along the steps 1 \rightarrow 2 \rightarrow 3 \rightarrow 4 of FIG. 4. Notice that for different h_1 values, WM radiates almost the same amount of heat to the cold bath, but the heat absorbed from the hot bath increases with an increase in h_1 , enhancing the efficiency substantially.

maximum at $J = -0.34$ and 0.295 , for $\kappa = \pm 1$, respectively. To understand the efficiency enhancement of KH system at some optimum combination of parameters, we compare the average energy calculated at any given point of the Otto cycle by plotting $\langle E(h_z(t)) \rangle = \text{Tr}(\rho(t)H(t))$ in FIG. 7(c,d) for $\kappa = \pm 1$, with respective J at which maximum efficiency occurs. From Eq.(3), the expression of efficiency reads as $\eta = 1 + (E^{(1)} - E^{(4)})/(E^{(3)} - E^{(2)})$, which indicates that the η is mainly determined by $E^{(1)}$ and $E^{(2)}$, as $E^{(3)}$ and $E^{(4)}$ do not change much for different J . Near the optimum efficiency delivering J points, Q_h attains a very low value while delivering a similar amount of work; this makes the efficiency to be enhanced substantially. At this optimum J , as we increase h_1 , the magnitude of $E^{(2)}$ increases while $E^{(3)}$ changes by a small amount, which directly enhances efficiency. The change in energy $E^{(1)} \rightarrow E^{(2)}$ and $E^{(3)} \rightarrow E^{(4)}$ actually denotes the energy released or absorbed by the system (in terms of work, to or from the external drive).

Realization of narrow bands and emergent magnons: Our numerical calculation reveals that for certain combinations of κ, J, h_z , the complete set of eigenstates along the unitary stroke remains quasi-stationary. Con-

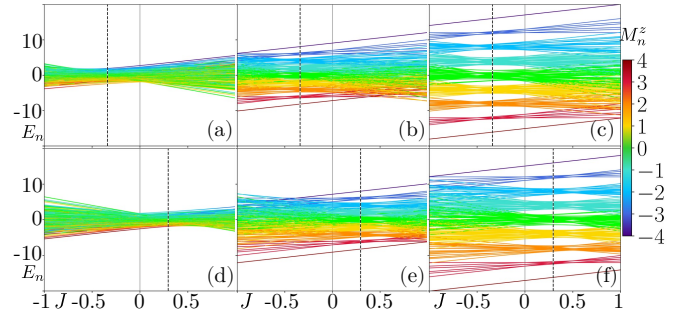


FIG. 8. Energy eigen-spectra plots for (a-c) AFM and (d-f) FM Kitaev model against J . The h_z values are 0.365 at (a), 0.31 at (d), 2.0 at (b,e), and 4.0 at (c,f). Black dotted line is at (a-c) $J = -0.34$, and (d-f) $J = +0.295$, corresponding to maximum efficiency delivering J points in AFM and FM Kitaev model respectively. Multiple narrow bands are formed around these dotted lines as one increases h_z . The color code in an eigen-energy denotes the total magnetization in \hat{z} -direction for that state. The number of bands is equal to the possible values of total magnetization, which turns out to be constant for a given band.

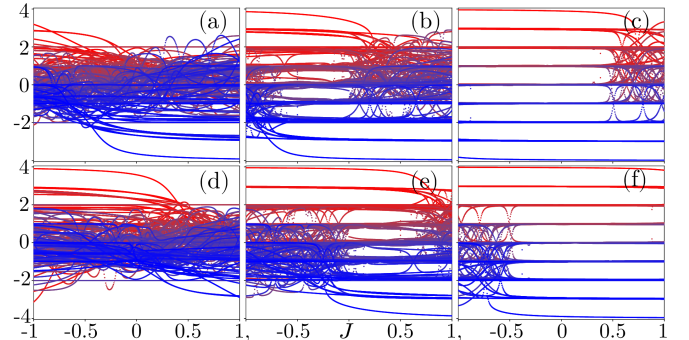


FIG. 9. Magnetization at each of the eigen-states for (a-c) AFM and (d-f) FM Kitaev model against J . The h_z values are 0.365 at (a), 0.31 at (d), 1.0 at (b,e), and 2.0 at (c,f). Pure red (■) and pure blue (■) represent the lowest and highest eigenstates' magnetization, and the color interpolates between these two for intermediate states.

comitantly, the eigenstates form multiple narrow bands as shown in [FIG. 8] and the number of bands equals the possible quantized values that the total S^z can take. This implies that for the 8-spin cluster, there should be nine bands, and our numerics exactly realize that. We infer this fact by investigating the eigenvalue spectrum and the expectation value of total magnetization denoted by $M_n^z := \langle n | \hat{M}_z | n \rangle = \langle n | \sum_{j=1}^N S_j^z | n \rangle$, calculated at $|n\rangle^{\text{th}}$ eigen-state. We see a gradual transition of the spectrum from continuous to a closely packed multiple narrow bands as one increases the value of the external magnetic field. The expectation values of M_z gradually evolve from arbitrary values to quantized values. In [FIG. 9], we plot the M^z values obtained, and it clearly demonstrates that in the region where narrow band formation occurs, magnetization values become

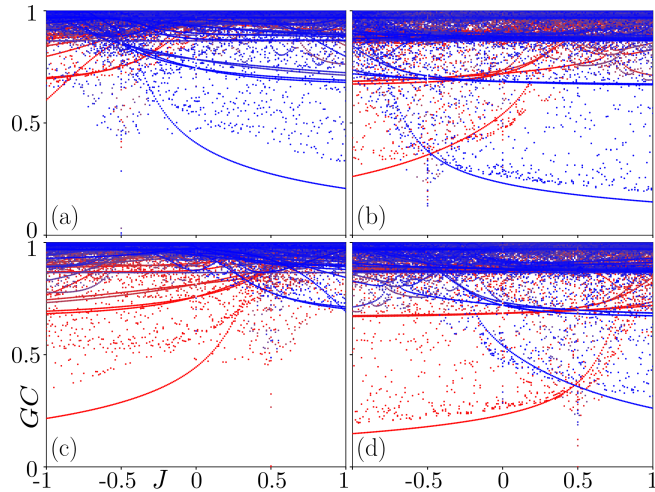


FIG. 10. The generalized concurrence (GC) for all eigenstates of the 8-site cluster is plotted. Pure red (■) and pure blue (■) represent the lowest and highest eigen-state concurrence, and the color interpolates between these two for intermediate states. The upper and lower panels represent AFM and FM κ , respectively. h_z is taken 0.365 at (a), 0.31 at (c), and 1.0 at (b,d).

quantized. It is known that when the magnetization is quantized exactly to the expected total S^z , it can be well described by magnons. Thus, our results point out another scenario where the emergent magnons play a crucial roles in maximizing the efficiency and offer another avenue of efficiency increasing mechanism in addition to adiabaticity [103, 104], or long range interactions [65]. Interestingly, we observe that the system exchanges more energy for such a scenario as established in panels (c) and (d) in FIG. 7.

Possible role of entanglement: We end this discussion with a possible role of entanglement contributing to observed results. The paths (1) \rightarrow (2) and (3) \rightarrow (4) of the Otto cycle are unitary, and the entanglement entropy does not change along these paths. There is a discontinuous jump in entropy from (2) \rightarrow (3) and (4) \rightarrow (1). It is interesting to note that entanglement entropy at point (1) (and (2)) follows a similar pattern as $E^{(1)}$ (and $E^{(2)}$) while varying J for fixed κ , h_2 , h_1 . Entropy at points (3) and (4) also follows a similar pattern as $E^{(3)}$ and $E^{(4)}$, but the magnitude is reduced due to the high temperature of the hot bath. Another fascinating observation is that the generalized concurrence [105] (a measure of entanglement for pure states) is symmetric [FIG. 10] in the KH system for similar combinations of $(\pm\kappa, \mp J)$, similar to what we observe in FIG. 7. Notice in FIG. 10(b,d), ground state concurrence is very close to that of the highest excited state, when we flip the sign of κ and J both. The QOE results are not exactly the same when we flip $(\pm\kappa, \mp J)$, because the response due to AFM and FM couplings is different in the presence of a magnetic field. QOE uses

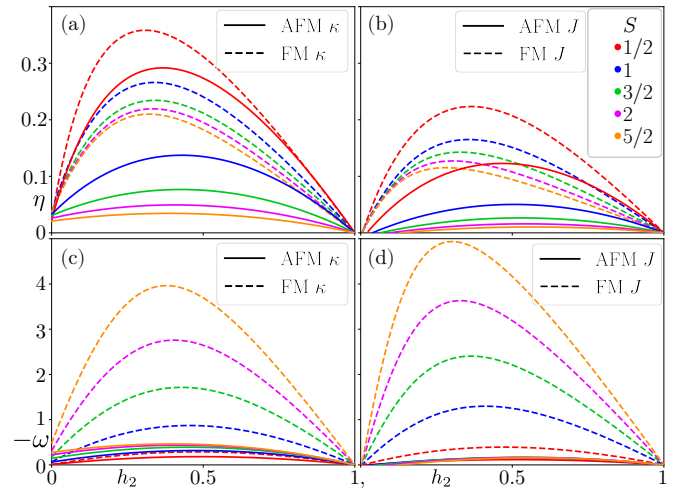


FIG. 11. (a,b) Efficiency η , and, (c,d) work $(-\omega)$ delivered by a spin- S heat-engine for the 4-site cluster. We have taken the WM to be a (a,c) pure Kitaev cluster with $|\kappa| = 1$, and (b,d) pure Heisenberg (tri-coordinated) cluster with $|J| = 1$. The parameter values are set at $(T_h, T_c, h_1) = (10^2, 10^0, 1)$, and h_2 varies from 0 \rightarrow h_1 . In all of the panels, different colors are for different spin sizes, as indicated in the legend box of (b).

the full energy spectra to determine its performance, and it is the concurrence of all states that is important. The entanglement results indicate a possible duality in the KH system for competing κ and J in the presence of a magnetic field, which shows its effect in determining the efficiency of QOE made with this WM.

C. Large- S heat-Engine

In recent years, many theoretical and experimental studies have been conducted for large spin- S Kitaev and KH models [106–113]. Theoretically, it offers a unique platform to study how strong quantum fluctuations realized for the QSL evolve as the magnitude of spin itself becomes larger [114]. This gives a direct way of measuring how a larger magnitude of S , known for weaker quantum fluctuation, competes with frustrations induced by interactions. Experimentally, there are also materials which propose the KH model with higher S [108]. There have been very few studies on QOE for either large spin or for multilevel systems with different dependency of efficiency on the magnitude of spin or the number of levels [115–120]. Here we briefly present the large- S QOE performance for the Kitaev model Hamiltonian considered in Eq.(1). The algebra of different components of large spin $\vec{S}(\{S_j^x, S_j^y, S_j^z\})$ now obey the commutations $[S_j^\alpha, S_j^\beta] = ie^{\alpha\beta\gamma} S_j^\gamma$ with a Hilbert space of dimension $(2S + 1)$ per spin [121]. As the exact diagonalization technique has been used, we restrict ourselves to $N = 4$ only.

In FIG. 11, we plot the efficiency and work output for different magnitudes of S (up to $S=5/2$). We observe that the FM Kitaev model yields better efficiency than the AFM one, for a given S . However, in both cases, the efficiency decreases with increasing S , thus showing evidence of quantum advantage. The work output for the FM Kitaev model is higher than the AFM one, and in both cases, it increases with S . To get an asymptotic dependency of efficiency and work, we fit the maximum of η and ω , with orders of S^{-1} . For AFM and FM Kitaev model, the maximum efficiency fits as $\eta_{\max} = 0.1615S^{-1} - 0.0295$, and $\eta_{\max} = 0.0928S^{-1} + 0.1729$, respectively. The maximum efficiency delivering points do not coincide with the maximum work producing h_2 values. The maximally produced work depends on S as, $-w_{\max} = 0.49(1 - \exp(-1.11(S - 0.09)))$ for AFM Kitaev model, and $-w_{\max} = -0.13 + 0.61S + 0.41S^2$ for the FM one. It is interesting that while an AFM Kitaev model gives a saturated value of work on increasing S , the FM Kitaev model yields a polynomial dependency.

In FIG. 11(c,d), we plot the efficiency and work of a pure Heisenberg model on the 4-site cluster. We observe that the same quantum advantage persists in efficiency, and there is a dimensional advantage in work. Interestingly, the Kitaev WM is much more efficient than the Heisenberg cluster, at the expense of a lesser disadvantage in work. This indicates the promising usefulness of the frustrated Kitaev system as compared to the Heisenberg model, in a quantum engine.

IV. CONCLUSION

We have investigated a quantum Otto engine with Kitaev-Heisenberg clusters serving as the many-body working medium. A time-dependent Zeeman field along the \hat{z} direction is taken as an external drive. A pure AFM or FM Kitaev model shows all four different modes the system can act as: heat-engine, refrigerator, heat-accelerator, and heater. Interestingly, the regions are almost cluster-size independent, which indicates the possible realization of similar results in larger Kitaev clusters too, which are computationally expensive. Heisenberg interaction added to either FM or AKM Kitaev model destroys the proximate-QSL regime to a varying degree, but it increases the efficiency only when the sign of a small J is opposite to that of κ . It possibly indicates that the proximate-QSL property is not the sole efficiency-determining factor. Neither does it depend on the simple quantum ordering mechanism between the working media and the external drive, as evident from the fact that for κ negative and J positive yields a better efficiency in comparison to J negative. Rather, it is the mutual quantum coherence between the external drive and the relative contribution from frustration and the collinear ordering that optimizes the efficiency. Our

work calls for a more in-depth analysis of this mechanism.

The present study uncovers a very subtle many-body effect of the Kitaev-Heisenberg system under a Zeeman field. The eigen-spectrum forms dense and narrow bands for a certain combination of signs and magnitude of J , κ , and h_z . Interestingly, when the working media dynamically enters these combinations of parameters, it realizes maximum efficiency. This connects the equilibrium property of the system to be a key efficiency-determining factor. The number of bands is equal to the quantized value of S_{total}^z , and the value is fixed at a particular band. The quantization of S_{total}^z indicates that the system can be effectively described by magnons, and it offers an interesting mechanism of weakly interacting magnons as an efficiency increasing mechanism. Further, we were able to characterize the various working modes by introducing the concept of fictitious effective temperature, which accounts for the energy exchange due to the external drive. Interestingly, this effective temperature also correctly captures the maximum efficiency where energy loss due to the external drive is minimized. Lastly, we have studied the heat-engine for a spin- S Kitaev cluster up to $S = 5/2$, and found a quantum advantage in efficiency, with $1/S$ dependency for both AFM and FM Kitaev models. The maximum work output exponentially saturates with increasing S for the AFM Kitaev model, whereas, it has a polynomial of second order dependency for the FM one. We expect that our study sheds new understanding on how the efficiency of a quantum engine depends crucially on multiple mechanisms such as competing interactions, frustrations, and duality of eigen-states, as well as emergent weakly interacting magnons. All of these facts act crucially to determine the engine performance for a many-spin system.

Given the recent interesting findings on the Kitaev-Heisenberg model [122], or Kitaev model under external Zeeman field [99], and other magnetic models with competing ground states [123, 124], our study calls for quantum engine studies in these systems to explore the effect of entanglement [125], dimensions [77] and other aspects. Further, it remains to see whether the results obtained for small Kitaev-Heisenberg clusters are also valid in the thermodynamic limit and the exact quantum factor optimizing the efficiency of such engines. Interestingly, in thermodynamic limit, the Kitaev model defined on higher dimensions [77], or in different lattices with gapless Fermi surface or line [126, 127], may be of interest to see dynamical effect of defect density [79, 128, 129] on quantum Otto engine and we leave it as future scope of study.

DATA AVAILABILITY STATEMENT

The data supporting this study's findings are available upon reasonable request from the corresponding author.

ACKNOWLEDGEMENT

The authors acknowledge valuable discussions with Victor Mukherjee. S.M.P. also thanks Soumya Bera, De-

bashish Mondal, and Ramita Sarkar for interesting discussions. Numerical calculations are partly performed in SAMKHYA (High-Performance Computing facility provided by the Institute of Physics, Bhubaneswar).

[1] C. L. Degen, F. Reinhard, and P. Cappellaro, Quantum sensing, *Rev. Mod. Phys.* **89**, 035002 (2017).

[2] R. Wiesendanger, Spin mapping at the nanoscale and atomic scale, *Rev. Mod. Phys.* **81**, 1495 (2009).

[3] Q. Bouton, J. Nettersheim, S. Burgardt, D. Adam, E. Lutz, and A. Widera, A quantum heat engine driven by atomic collisions, *Nature Communications* **12**, 2063 (2021).

[4] R. Kosloff and A. Levy, Quantum heat engines and refrigerators: Continuous devices, *Annual Review of Physical Chemistry* **65**, 365 (2014).

[5] S. Bandyopadhyay, S. Laha, U. Bhattacharya, and A. Dutta, Exploring the possibilities of dynamical quantum phase transitions in the presence of a markovian bath, *Scientific Reports* **8**, 11921 (2018).

[6] N. Jaseem, S. Vinjanampathy, and V. Mukherjee, Quadratic enhancement in the reliability of collective quantum engines, *Phys. Rev. A* **107**, L040202 (2023).

[7] T. K. Konar, S. Ghosh, A. K. Pal, and A. Sen(De), Designing robust quantum refrigerators in disordered spin models, *Phys. Rev. A* **105**, 022214 (2022).

[8] E. Muñoz, F. J. Peña, and A. González, Magnetically-driven quantum heat engines: The quasi-static limit of their efficiency, *Entropy* **18**, 10.3390/e18050173 (2016).

[9] R. B. S. V. Mukherjee, U. Divakaran, and A. del Campo, Universal finite-time thermodynamics of many-body quantum machines from kibble-zurek scaling, *Phys. Rev. Res.* **2**, 043247 (2020).

[10] D. Manzano, A short introduction to the lindblad master equation, *AIP Advances* **10**, 10.1063/1.5115323 (2020).

[11] T. K. Konar, A. Patra, R. Gupta, S. Ghosh, and A. Sen(De), Multimode advantage in continuous-variable quantum batteries, *Phys. Rev. A* **110**, 022226 (2024).

[12] S. Ghosh and A. Sen(De), Dimensional enhancements in a quantum battery with imperfections, *Phys. Rev. A* **105**, 022628 (2022).

[13] T. K. Konar, L. G. C. Lakkaraju, and A. Sen (De), Quantum battery with non-hermitian charging, *Phys. Rev. A* **109**, 042207 (2024).

[14] S. Ghosh, T. Chanda, S. Mal, and A. Sen(De), Fast charging of a quantum battery assisted by noise, *Phys. Rev. A* **104**, 032207 (2021).

[15] F. Binder, L. A. Correa, C. Gogolin, J. Anders, and G. Adesso, *Thermodynamics in the Quantum Regime*, Fundamental Theories of Physics, Vol. 195 (Springer International Publishing, New York, 2018).

[16] C. Jarzynski, Nonequilibrium equality for free energy differences, *Phys. Rev. Lett.* **78**, 2690 (1997).

[17] M. Campisi, P. Hänggi, and P. Talkner, Colloquium: Quantum fluctuation relations: Foundations and applications, *Rev. Mod. Phys.* **83**, 771 (2011).

[18] J. Åberg, Fully quantum fluctuation theorems, *Phys. Rev. X* **8**, 011019 (2018).

[19] F. G. S. L. Brandão, M. Horodecki, J. Oppenheim, J. M. Renes, and R. W. Spekkens, Resource theory of quantum states out of thermal equilibrium, *Phys. Rev. Lett.* **111**, 250404 (2013).

[20] W. Niedenzu, V. Mukherjee, A. Ghosh, A. G. Kofman, and G. Kurizki, Quantum engine efficiency bound beyond the second law of thermodynamics, *Nature Communications* **9**, 165 (2018).

[21] D. D'Alessandro, *Introduction to Quantum Control and Dynamics*, Applied Mathematics and Nonlinear Science Series (Chapman & Hall/CRC, Boca Raton, 2008).

[22] M. A. Nielsen and I. L. Chuang, *Quantum Computation and Quantum Information: 10th Anniversary Edition* (Cambridge University Press, Cambridge, 2010).

[23] T. Konrad, A. Rouillard, M. Kastner, and H. Uys, Robust control of quantum systems by quantum systems, *Phys. Rev. A* **104**, 052614 (2021).

[24] J. Wechs, H. Dourdent, A. A. Abbott, and C. Branciard, Quantum circuits with classical versus quantum control of causal order, *PRX Quantum* **2**, 030335 (2021).

[25] M. Contreras González, M. Villena, and R. Ortiz Herrera, An optimal control perspective on classical and quantum physical systems, *Symmetry* **15**, 10.3390/sym15112033 (2023).

[26] G. Gour, D. Jennings, F. Buscemi, R. Duan, and I. Marvian, Quantum majorization and a complete set of entropic conditions for quantum thermodynamics, *Nature Communications* **9**, 5352 (2018).

[27] H. E. D. Scovil and E. O. Schulz-DuBois, Three-level masers as heat engines, *Phys. Rev. Lett.* **2**, 262 (1959).

[28] J. E. Geusic, E. O. Schulz-DuBios, and H. E. D. Scovil, Quantum equivalent of the carnot cycle, *Phys. Rev.* **156**, 343 (1967).

[29] M. Horodecki and J. Oppenheim, Fundamental limitations for quantum and nanoscale thermodynamics, *Nature Communications* **4**, 2059 (2013).

[30] P. Skrzypczyk, A. J. Short, and S. Popescu, Work extraction and thermodynamics for individual quantum systems, *Nature Communications* **5**, 4185 (2014).

[31] F. Brandão, M. Horodecki, N. Ng, J. Oppenheim, and S. Wehner, The second laws of quan-

tum thermodynamics, *Proceedings of the National Academy of Sciences* **112**, 3275 (2015), <https://www.pnas.org/doi/pdf/10.1073/pnas.1411728112>.

[32] M. Lostaglio, D. Jennings, and T. Rudolph, Description of quantum coherence in thermodynamic processes requires constraints beyond free energy, *Nature Communications* **6**, 6383 (2015).

[33] M. P. Müller, Correlating thermal machines and the second law at the nanoscale, *Phys. Rev. X* **8**, 041051 (2018).

[34] R. Uzdin and S. Rahav, Global passivity in microscopic thermodynamics, *Phys. Rev. X* **8**, 021064 (2018).

[35] J. Arnaud, L. Chusseau, and F. Philippe, A simple quantum heat engine (2003), [arXiv:quant-ph/0211072 \[quant-ph\]](https://arxiv.org/abs/quant-ph/0211072).

[36] T. D. Kieu, The second law, maxwell's demon, and work derivable from quantum heat engines, *Phys. Rev. Lett.* **93**, 140403 (2004).

[37] T. Chowdhury, A. Rosch, and R. Bulla, Competition between kondo physics and kitaev physics in kitaev clusters coupled to a fermionic bath, *Phys. Rev. B* **101**, 115133 (2020).

[38] S. M. Pervez and S. Mandal, Deciphering competing interactions of kitaev–heisenberg– γ system in clusters: I. static properties, *Journal of Physics: Condensed Matter* **37**, 025802 (2024).

[39] S. M. Pervez and S. Mandal, Deciphering competing interactions of kitaev–heisenberg– γ system in clusters: II. dynamics of majorana fermions, *Journal of Physics: Condensed Matter* **37**, 025803 (2024).

[40] K. Kataoka, D. Hirai, T. Yajima, D. Nishio-Hamane, R. Ishii, K.-Y. Choi, D. Wulferding, P. Lemmens, S. Kittaka, T. Sakakibara, H. Ishikawa, A. Matsuo, K. Kindo, and Z. Hiroi, Kitaev spin liquid candidate oxcl3 comprised of honeycomb nano-domains, *Journal of the Physical Society of Japan* **89**, 114709 (2020), <https://doi.org/10.7566/JPSJ.89.114709>.

[41] E. M. Wilson, J.-X. Zhu, and J. T. Haraldsen, Exact eigenvalues and experimental signatures of heisenberg–kitaev interactions in spin-1/2 quantum clusters (2025), [arXiv:2506.06967 \[cond-mat.mtrl-sci\]](https://arxiv.org/abs/2506.06967).

[42] H. T. Quan, Y.-x. Liu, C. P. Sun, and F. Nori, Quantum thermodynamic cycles and quantum heat engines, *Phys. Rev. E* **76**, 031105 (2007).

[43] J. Heywood, *Internal Combustion Engine Fundamentals* (McGraw-Hill Education, 2018).

[44] C. P. P. Hill, *Mechanics and Thermodynamics of Propulsion* (Pearson, 1991).

[45] R. Stone, *Introduction to Internal Combustion Engines* (M. Macmillan, 1985).

[46] T. Kroetz, Revisiting and comparing the carnot cycle and the otto cycle, *Revista Brasileira de Ensino de Física* **46**, e20230318 (2024).

[47] T. Feldmann and R. Kosloff, Quantum four-stroke heat engine: Thermodynamic observables in a model with intrinsic friction, *Phys. Rev. E* **68**, 016101 (2003).

[48] H. T. Quan, P. Zhang, and C. P. Sun, Quantum heat engine with multilevel quantum systems, *Phys. Rev. E* **72**, 056110 (2005).

[49] H. T. Quan, Y. D. Wang, Y.-x. Liu, C. P. Sun, and F. Nori, Maxwell's demon assisted thermodynamic cycle in superconducting quantum circuits, *Phys. Rev. Lett.* **97**, 180402 (2006).

[50] Y. Rezek and R. Kosloff, Irreversible performance of a quantum harmonic heat engine, *New Journal of Physics* **8**, 83 (2006).

[51] T. Feldmann, E. Geva, R. Kosloff, and P. Salamon, Heat engines in finite time governed by master equations, *American Journal of Physics* **64**, 485 (1996).

[52] E. Geva and R. Kosloff, A quantum-mechanical heat engine operating in finite time. a model consisting of spin-1/2 systems as the working fluid, *The Journal of Chemical Physics* **96**, 3054 (1992).

[53] R. Kosloff and Y. Rezek, The quantum harmonic otto cycle, *Entropy* **19**, 10.3390/e19040136 (2017).

[54] A. Şışman and H. Saygin, Re-optimisation of otto power cycles working with ideal quantum gases, *Physica Scripta* **64**, 108 (2001).

[55] J. Chen, H. Dong, and C.-P. Sun, Bose-fermi duality in a quantum otto heat engine with trapped repulsive bosons, *Phys. Rev. E* **98**, 062119 (2018).

[56] H. Wang, S. Liu, and J. He, Performance analysis and parametric optimum criteria of a quantum otto heat engine with heat transfer effects, *Applied Thermal Engineering* **29**, 706 (2009).

[57] H. Wang, S. Liu, and J. He, Performance analysis and parametric optimum criteria of an irreversible bose–otto engine, *Journal of Applied Physics* **105**, 083534 (2009).

[58] H. T. Quan, Quantum thermodynamic cycles and quantum heat engines. ii., *Phys. Rev. E* **79**, 041129 (2009).

[59] R. S. Johal and V. Mehta, Quantum heat engines with complex working media, complete otto cycles and heuristics, *Entropy* **23**, 10.3390/e23091149 (2021).

[60] K.-W. Sun, C. Wang, and Q.-H. Chen, Heat transport in an open transverse-field ising chain, *Europhysics Letters* **92**, 24002 (2010).

[61] G. Piccitto, M. Campisi, and D. Rossini, The ising critical quantum otto engine, *New Journal of Physics* **24**, 103023 (2022).

[62] M. Asadian, S. Ahadpour, and F. Mirmasoudi, Quantum correlated heat engine in xy chain with dzyaloshinskii–moriya interactions, *Scientific Reports* **12**, 7081 (2022).

[63] E. I. Kuznetsova, M. A. Yurishev, and S. Haddadi, Quantum otto heat engines on xyz spin working medium with dm and ksea interactions: operating modes and efficiency at maximal work output, *Quantum Information Processing* **22**, 192 (2023).

[64] Q. Wang, Performance of quantum heat engines under the influence of long-range interactions, *Phys. Rev. E* **102**, 012138 (2020).

[65] A. Solfanelli, G. Giachetti, M. Campisi, S. Ruffo, and N. Defenu, Quantum heat engine with long-range advantages, *New Journal of Physics* **25**, 033030 (2023).

[66] E. Yunt, M. Fadaie, O. E. Müstecaplıoğlu, and C. M. Smith, Internal geometric friction in a kitaev-chain heat engine, *Phys. Rev. B* **102**, 155423 (2020).

[67] E. Yunt, M. Fadaie, and Özgür E. Müstecaplıoğlu, *Topological and finite size effects in a kitaev chain heat engine* (2019), [arXiv:1908.02643 \[cond-mat.stat-mech\]](https://arxiv.org/abs/1908.02643).

[68] R. J. de Assis, T. M. de Mendonça, C. J. Villas-Boas, A. M. de Souza, R. S. Sarthour, I. S. Oliveira, and N. G. de Almeida, Efficiency of a quantum otto heat engine operating under a reservoir at effective negative temperatures, *Phys. Rev. Lett.* **122**, 240602 (2019).

[69] J. P. S. Peterson, T. B. Batalhão, M. Herrera, A. M. Souza, R. S. Sarthour, I. S. Oliveira, and R. M. Serra, Experimental characterization of a spin quantum heat

engine, *Phys. Rev. Lett.* **123**, 240601 (2019).

[70] A. Sofanelli, M. Falsetti, and M. Campisi, Nonadiabatic single-qubit quantum otto engine, *Phys. Rev. B* **101**, 054513 (2020).

[71] A. Maity and A. S. De, Enhanced efficiency in quantum otto engine via additional magnetic field and effective negative temperature (2023), arXiv:2304.10420 [quant-ph].

[72] L. Balents, Spin liquids in frustrated magnets, *Nature* **464**, 199 (2010).

[73] L. Savary and L. Balents, Quantum spin liquids: a review, *Reports on Progress in Physics* **80**, 016502 (2016).

[74] S. Mandal, R. Shankar, and G. Baskaran, Rvb gauge theory and the topological degeneracy in the honeycomb kitaev model, *Journal of Physics A: Mathematical and Theoretical* **45**, 335304 (2012).

[75] A. Kitaev, Anyons in an exactly solved model and beyond, *Annals of Physics* **321**, 2 (2006), january Special Issue.

[76] S. Mandal, A primer on kitaev model: basic aspects, material realization, and recent experiments, *Journal of Physics: Condensed Matter* **37**, 193002 (2025).

[77] S. Mandal and N. Surendran, Exactly solvable kitaev model in three dimensions, *Phys. Rev. B* **79**, 024426 (2009).

[78] S. Mandal and N. Surendran, Fermions and nontrivial loop-braiding in a three-dimensional toric code, *Phys. Rev. B* **90**, 104424 (2014).

[79] S. Sarkar, D. Rana, and S. Mandal, Defect production and quench dynamics in the three-dimensional kitaev model, *Phys. Rev. B* **102**, 134309 (2020).

[80] T. Eschmann, P. A. Mishchenko, K. O'Brien, T. A. Bojesen, Y. Kato, M. Hermanns, Y. Motome, and S. Trebst, Thermodynamic classification of three-dimensional kitaev spin liquids, *Phys. Rev. B* **102**, 075125 (2020).

[81] G. Jackeli and G. Khaliullin, Mott insulators in the strong spin-orbit coupling limit: From heisenberg to a quantum compass and kitaev models, *Phys. Rev. Lett.* **102**, 017205 (2009).

[82] M. Hermanns, I. Kimchi, and J. Knolle, Physics of the kitaev model: Fractionalization, dynamic correlations, and material connections, *Annual Review of Condensed Matter Physics* **9**, 17 (2018).

[83] J. G. Rau, E. K.-H. Lee, and H.-Y. Kee, Spin-orbit physics giving rise to novel phases in correlated systems: Iridates and related materials, *Annual Review of Condensed Matter Physics* **7**, 195 (2016).

[84] S. Trebst and C. Hickey, Kitaev materials, *Physics Reports* **950**, 1 (2022), kitaev materials.

[85] H. Takagi, T. Takayama, G. Jackeli, G. Khaliullin, and S. E. Nagler, Concept and realization of kitaev quantum spin liquids, *Nature Reviews Physics* **1**, 264 (2019).

[86] Y. Motome, R. Sano, S. Jang, Y. Sugita, and Y. Kato, Materials design of kitaev spin liquids beyond the jackeli-khaliullin mechanism, *Journal of Physics: Condensed Matter* **32**, 404001 (2020).

[87] M. Hermanns, I. Kimchi, and J. Knolle, Physics of the kitaev model: Fractionalization, dynamic correlations, and material connections, *Annual Review of Condensed Matter Physics* **9**, 17 (2018), <https://doi.org/10.1146/annurev-conmatphys-033117-053934>.

[88] A. Banerjee, C. A. Bridges, J.-Q. Yan, A. A. Aczel, L. Li, M. B. Stone, G. E. Granroth, M. D. Lumsden, Y. Yiu, J. Knolle, S. Bhattacharjee, D. L. Kovrizhin, R. Moessner, D. A. Tennant, D. G. Mandrus, and S. E. Nagler, Proximate kitaev quantum spin liquid behaviour in a honeycomb magnet, *Nature Materials* **15**, 733 (2016).

[89] A. Banerjee, J. Yan, J. Knolle, C. A. Bridges, M. B. Stone, M. D. Lumsden, D. G. Mandrus, D. A. Tennant, R. Moessner, and S. E. Nagler, Neutron scattering in the proximate quantum spin liquid α -rucl₃, *Science* **356**, 1055 (2017).

[90] H. Gretarsson, J. P. Clancy, X. Liu, J. P. Hill, E. Bozin, Y. Singh, S. Manni, P. Gegenwart, J. Kim, A. H. Said, D. Casa, T. Gog, M. H. Upton, H.-S. Kim, J. Yu, V. M. Katukuri, L. Hozoi, J. van den Brink, and Y.-J. Kim, Crystal-field splitting and correlation effect on the electronic structure of A_2 iro₃, *Phys. Rev. Lett.* **110**, 076402 (2013).

[91] S. K. Choi, R. Coldea, A. N. Kolmogorov, T. Lancaster, I. I. Mazin, S. J. Blundell, P. G. Radaelli, Y. Singh, P. Gegenwart, K. R. Choi, S.-W. Cheong, P. J. Baker, C. Stock, and J. Taylor, Spin waves and revised crystal structure of honeycomb iridate Na_2 iro₃, *Phys. Rev. Lett.* **108**, 127204 (2012).

[92] T. Takayama, A. Kato, R. Dinnebier, J. Nuss, H. Kono, L. S. I. Veiga, G. Fabbris, D. Haskel, and H. Takagi, Hyperhoneycomb iridate β -li₂iro₃ as a platform for kitaev magnetism, *Phys. Rev. Lett.* **114**, 077202 (2015).

[93] Y. Singh, S. Manni, J. Reuther, T. Berlijn, R. Thomale, W. Ku, S. Trebst, and P. Gegenwart, Relevance of the heisenberg-kitaev model for the honeycomb lattice iridates A_2 iro₃, *Phys. Rev. Lett.* **108**, 127203 (2012).

[94] D. C. Ronquillo, A. Vengal, and N. Trivedi, Signatures of magnetic-field-driven quantum phase transitions in the entanglement entropy and spin dynamics of the kitaev honeycomb model, *Phys. Rev. B* **99**, 140413 (2019).

[95] Z. Zhu, I. Kimchi, D. N. Sheng, and L. Fu, Robust non-abelian spin liquid and a possible intermediate phase in the antiferromagnetic kitaev model with magnetic field, *Phys. Rev. B* **97**, 241110 (2018).

[96] J. Nasu, Y. Kato, Y. Kamiya, and Y. Motome, Successive majorana topological transitions driven by a magnetic field in the kitaev model, *Phys. Rev. B* **98**, 060416 (2018).

[97] S. Pradhan, N. D. Patel, and N. Trivedi, Two-magnon bound states in the kitaev model in a [111] field, *Phys. Rev. B* **101**, 180401 (2020).

[98] S. Feng, A. Agarwala, S. Bhattacharjee, and N. Trivedi, Anyon dynamics in field-driven phases of the anisotropic kitaev model, *Phys. Rev. B* **108**, 035149 (2023).

[99] K. B. Yogendra, T. Das, and G. Baskaran, Emergent glassiness in the disorder-free kitaev model: Density matrix renormalization group study on a one-dimensional ladder setting, *Phys. Rev. B* **108**, 165118 (2023).

[100] L. Lyu, D. Chandorkar, S. Kapoor, S. Takei, E. S. Sørensen, and W. Witczak-Krempa, Multiparty entanglement loops in quantum spin liquids (2025), arXiv:2505.18124 [cond-mat.str-el].

[101] G. Baskaran, S. Mandal, and R. Shankar, Exact results for spin dynamics and fractionalization in the kitaev model, *Phys. Rev. Lett.* **98**, 247201 (2007).

[102] C. Hickey and S. Trebst, Emergence of a field-driven $u(1)$ spin liquid in the kitaev honeycomb model, *Nature*

Communications **10**, 530 (2019).

[103] A. Hartmann, V. Mukherjee, W. Niedenzu, and W. Lechner, Many-body quantum heat engines with shortcuts to adiabaticity, *Phys. Rev. Res.* **2**, 023145 (2020).

[104] T. Feldmann and R. Kosloff, Quantum lubrication: Suppression of friction in a first-principles four-stroke heat engine, *Phys. Rev. E* **73**, 025107 (2006).

[105] S. Dutta, R. Sarkar, and P. K. Panigrahi, Permutation symmetric hypergraph states and multipartite quantum entanglement, *International Journal of Theoretical Physics* **58**, 3927 (2019).

[106] H. Ma, F_2 spin liquids in the higher spin- s kitaev honeycomb model: An exact deconfined F_2 gauge structure in a nonintegrable model, *Phys. Rev. Lett.* **130**, 156701 (2023).

[107] P. P. Stavropoulos, D. Pereira, and H.-Y. Kee, Microscopic mechanism for a higher-spin kitaev model, *Phys. Rev. Lett.* **123**, 037203 (2019).

[108] C. Xu, J. Feng, M. Kawamura, Y. Yamaji, Y. Nahas, S. Prokhorenko, Y. Qi, H. Xiang, and L. Bellaiche, Possible kitaev quantum spin liquid state in 2d materials with $s = 3/2$, *Phys. Rev. Lett.* **124**, 087205 (2020).

[109] J. Cen and H.-Y. Kee, Determining kitaev interaction in spin- s honeycomb mott insulators, *Phys. Rev. B* **107**, 014411 (2023).

[110] G. Baskaran, D. Sen, and R. Shankar, Spin- s kitaev model: Classical ground states, order from disorder, and exact correlation functions, *Phys. Rev. B* **78**, 115116 (2008).

[111] J. Oitmaa, A. Koga, and R. R. P. Singh, Incipient and well-developed entropy plateaus in spin- s kitaev models, *Phys. Rev. B* **98**, 214404 (2018).

[112] A. Koga, H. Tomishige, and J. Nasu, Ground-state and thermodynamic properties of an $s = 1$ kitaev model, *Journal of the Physical Society of Japan* **87**, 063703 (2018).

[113] Z. Zhu, Z.-Y. Weng, and D. N. Sheng, Magnetic field induced spin liquids in $s = 1$ kitaev honeycomb model, *Phys. Rev. Res.* **2**, 022047 (2020).

[114] P. M. Cónsoli, L. Janssen, M. Vojta, and E. C. Andrade, Heisenberg-kitaev model in a magnetic field: 1/ s expansion, *Phys. Rev. B* **102**, 155134 (2020).

[115] A. Hartmann, V. Mukherjee, G. B. Mbeng, W. Niedenzu, and W. Lechner, Multi-spin counter-diabatic driving in many-body quantum Otto refrigerators, *Quantum* **4**, 377 (2020).

[116] J. Nettersheim, S. Burgardt, Q. Bouton, D. Adam, E. Lutz, and A. Widera, Power of a quasispin quantum otto engine at negative effective spin temperature, *PRX Quantum* **3**, 040334 (2022).

[117] Q. Bouton, J. Nettersheim, S. Burgardt, D. Adam, E. Lutz, and A. Widera, A quantum heat engine driven by atomic collisions, *Nature Communications* **12**, 2063 (2021).

[118] M. A. Aguilera, F. J. Peña, O. A. Negrete, and P. Vargas, Otto engine for the q-state clock model, *Entropy* **24**, 10.3390/e24020268 (2022).

[119] F. Altintas and O. E. Müstecaplıoğlu, General formalism of local thermodynamics with an example: Quantum otto engine with a spin-1/2 coupled to an arbitrary spin, *Phys. Rev. E* **92**, 022142 (2015).

[120] Y. Hong, Y. Xiao, J. He, and J. Wang, Quantum otto engine working with interacting spin systems: Finite power performance in stochastic thermodynamics, *Phys. Rev. E* **102**, 022143 (2020).

[121] S. S. Jahromi, M. Hörmann, P. Adelhardt, S. Fey, H. Karamnejad, R. Orús, and K. P. Schmidt, Kitaev honeycomb antiferromagnet in a field: quantum phase diagram for general spin, *Communications Physics* **7**, 319 (2024).

[122] M. Routh, S. Ghosh, J. van den Brink, S. Nishimoto, and M. Kumar, Emergent quadrupolar order in the spin- $\frac{1}{2}$ kitaev-heisenberg model, *Phys. Rev. B* **109**, L220403 (2024).

[123] A. Maity, Y. Iqbal, and S. Mandal, Competing orders in a frustrated heisenberg model on the fisher lattice, *Phys. Rev. B* **102**, 224404 (2020).

[124] A. Maity, F. Ferrari, R. Thomale, S. Mandal, and Y. Iqbal, Projective symmetry group classification of abrikosov fermion mean-field ansätze on the square-octagon lattice, *Phys. Rev. B* **107**, 134438 (2023).

[125] S. Mandal, M. Maiti, and V. K. Varma, Entanglement and majorana edge states in the kitaev model, *Phys. Rev. B* **94**, 045421 (2016).

[126] M. G. Yamada, Topological Z_2 invariant in kitaev spin liquids: Classification of gapped spin liquids beyond projective symmetry group, *Phys. Rev. Res.* **3**, L012001 (2021).

[127] G. Kells, J. Kailasvuori, J. K. Slingerland, and J. Vala, Kaleidoscope of topological phases with multiple majorana species, *New Journal of Physics* **13**, 095014 (2011).

[128] K. Sengupta, D. Sen, and S. Mondal, Exact results for quench dynamics and defect production in a two-dimensional model, *Phys. Rev. Lett.* **100**, 077204 (2008).

[129] S. Mondal, D. Sen, and K. Sengupta, Quench dynamics and defect production in the kitaev and extended kitaev models, *Phys. Rev. B* **78**, 045101 (2008).